Kati Miettunen, Janne Halme, Paula Vahermaa, Tapio Saukkonen, Minna Toivola, and Peter Lund. 2009. Dye solar cells on ITO-PET substrate with TiO_2 recombination blocking layers. Journal of The Electrochemical Society, volume 156, number 8, pages B876-B883.

Journal of The Electrochemical Society, **156** (8) B876-B883 (2009)
0013-4651/2009/156(8)/B876/8/$25.00 © The Electrochemical Society

Dye Solar Cells on ITO-PET Substrate with TiO_2 Recombination Blocking Layers

Kati Miettunen,[a,z] Janne Halme,[a] Paula Vahermaa,[a] Tapio Saukkonen,[b] Minna Toivola,[a] and Peter Lund[a]

[a]*Advanced Energy Systems, Department of Applied Physics and* [b]*Engineering Materials Group, Department of Engineering Design and Production, Helsinki University of Technology, Espoo FIN-02015 TKK, Finland*

Atomic-layer-deposited TiO_2 recombination blocking layers were prepared on indium tin oxide–poly(ethylene terephthalate) (ITO–PET) photoelectrode substrates for dye solar cells and were examined using several electrochemical methods. The blocking layers increased the open-circuit voltage at low light intensities. At high light intensities, a decrease in the fill factor (FF) due to the additional resistance of the current transport through the layer was more significant than the positive effect by the reduced recombination. The decrease in the FF was reduced by a thermal treatment that made the blocking layer more conductive due to a structural change from an amorphous to a crystalline form. Therefore, thinner blocking layers of this type are required for plastic cells prepared at low temperature than for conventional glass dye solar cells made with temperature processing.
 [DOI: 10.1149/1.3138129]

Manuscript submitted December 15, 2008; revised manuscript received March 30, 2009. Published May 28, 2009.

Nanostructured dye solar cells (DSCs) have traditionally been deposited on fluorine-doped tin oxide (FTO) glass sheets. Different plastic and metal substrates have been investigated in recent years to decrease material costs and to advance suitability for roll to roll mass production. Plastic sheets have the advantage of being lightweight and flexible. They can also offer adequate transparency contrary to metals. Flexible DSCs are therefore commonly based either solely[1,2] or partly on polymer substrates with a conductive layer of indium tin oxide (ITO).[3-5] Several low temperature (LT) methods have been presented to prepare both the photoactive and the catalyst layers.

An optimal DSC substrate has high transparency, low sheet resistance, and good stability. It also acts as a physical barrier to moisture penetration and the leakage of the liquid electrolyte and provides mechanical support to the cell structure. An optimal photoelectrode (PE) substrate forms a low resistance Ohmic contact with the TiO_2 nanoparticle film but effectively blocks electron transfer to the oxidized species (usually tri-iodide) in the electrolyte. This so-called recombination from the substrate has predominantly been studied in FTO-coated glass substrates.[6-13] Only recently, other materials such as stainless steel have been examined.[11] To reduce the recombination losses, the use of blocking layers has been introduced.[6,8-10,13]

It has been detected that recombination losses via the substrate are especially significant at low light intensities.[6,7,12] DSCs on glass are typically designed to be used in building integrated photovoltaic systems in which case they are designed for high light intensities. However, the lightweight plastic solar cells are considered to be suitable for portable applications typically used indoors in low light intensity conditions. Maintaining a high open-circuit voltage by the suppression of the substrate-mediated recombination is therefore an essential requirement for plastic DSCs.

Here, the electrochemical performance of an ITO-coated polymer sheet as the PE substrate is examined in comparison to FTO glass substrates. We compared two commercially interesting DSC PE technologies, flexible and rigid. The effect of atomic-layer-deposited (ALD) TiO_2 blocking layers is studied as well. Two very different values for the ALD TiO_2 layer thickness were tested to determine the suitable order of magnitude for it. In literature the effect of blocking layers on the open-circuit voltage and the fill factor (FF) varied considerably.[6,8-10] Therefore a thorough and critical analysis is motivated to disaggregate the different ways these blocking layers contribute to the photovoltaic performance of the cell. In the analysis several complementary techniques were used: substrate polarization, open-circuit voltage decay (OCVD), and electrochemical impedance spectroscopy (EIS). The results from these methods are compared and contrasted with the photovoltaic performance of the solar cells.

[z] E-mail: kati.miettunen@tkk.fi

Experimental

Samples.— In this study, we compared two types of solar cells: first, the PE was prepared by a LT compression method,[14] and second, a conventional PE on an FTO glass substrate was prepared using high temperature (HT) sintering of a commercial TiO_2 paste. Solar cells with the low temperature pressed PE on FTO glass were prepared to separate the effect of the substrate from other factors. In addition to the complete solar cells, substrate–counter electrode (SU–CE) cells were made. The substrates of the SU–CE cells were thermally treated and dyed in a similar fashion as the PEs to ensure the resemblance to the PE substrate in the solar cell. The solar cell structure was not optimized for maximum efficiency.

The studied substrates were ITO–polyethylene terephthalate (PET) (NV-CT-CH-1S-M-7, 60 Ω/□, 200 μm, Bekaert Specialty Films, Inc.) and FTO glass (TEC-15, 15 Ω/□, 2.5 mm, Pilkington, Hartford Glass Co., Inc.). The substrates were washed with a mild detergent followed by an ultrasonic bath for 3 min first in ethanol and then in acetone. The atomic layer deposition of the TiO_2 blocking layers was prepared at 100°C by Planar Inc. The deposited film thicknesses were aimed for 5 and 50 nm, and the resulting films were specified to be 4 and 35 nm based on ellipsometry using a silicon reference.

Three kinds of PEs were made: pressed PEs on both ITO–PET and FTO glass and sintered PEs solely on FTO glass. The pressed/LT-treated PEs were made by doctor-blading a solution of 20 wt % TiO_2 (P25, Degussa) in ethanol, followed by compressing at ca. 700 kg/cm^2. The PE was covered with a poly(tetrafluoroethylene) foil during the pressing. The ready-made pressed layers were heated at 120°C before dye sensitization. The sintered/HT-treated porous TiO_2 layers were deposited by doctor-blading a commercial TiO_2 paste (Sustainable Technologies International) followed by drying at 120°C and sintering at 450°C for 30 min. A mask tape (3M scotch removable tape, thickness 65 μm) with a hole of 4 × 8 mm was employed in the distribution of both TiO_2 pastes. The TiO_2 layer thickness was typically ca. 15 μm measured with a Dektak 6M profiler. The TiO_2 layers were sensitized for 16 h in an N-719 dye solution consisting of 0.32 mM *cis*-bis(isothiocyanato) bis(2,2′-bipyridyl-4,4′-dicarboxylato)-ruthenium(II) bis-tetrabutylammonium (Solaronix) in absolute ethanol.

The counter electrodes were prepared on FTO glass substrates using thermal deposition from a platinum precursor solution consist-

ing of 5 mM $PtCl_4$ (Sigma-Aldrich) dissolved in 2-propanol and heating at 385°C for 15 min.[15] Typically, the electrolyte contained 0.5 M LiI, 0.03 M I_2, and 0.05 M 4-*tert*-butylpyridine in 3-methoxypropionitrile, and 25 μm thick Surlyn 1702 ionomer resin film spacers were used. Some of the pressed electrodes on ITO–PET were prepared with a thicker layer of TiO_2 (24–30 μm) in which case two spacer foils were used instead of one and the I_2 concentration was increased to 0.05 M to reach the same limiting current.

The electrolyte was inserted through filling holes in the counter electrode, which were sealed with a 40 μm thick Surlyn 1601 film and a thin cover glass. Copper tapes served as current collector contacts. Electrolube conducting silver paint was applied on the interface of the substrate and the tape to reduce resistance.

Measurements.— Photovoltaic measurements were performed using a solar simulator constructed of halogen lamps providing 1 sun (1000 W/m^2 AM1.5G) equivalent light intensity determined by a calibrated silicon reference cell with a spectral filter to mimic a typical DSC response. The solar cells were placed on a black surface cooled to 25°C with Peltier elements. The current–voltage (*I-V*) curves were measured using a Keithley 2420 SourceMeter. The ready-made solar cells were provided with black masks with a slightly larger aperture compared to the active area of the cell.[16]

The *I-V* measurements at low light intensities were made in a black box with a red light-emitting diode (LED) (λ_{peak} = 639 nm) as the light source. The light intensity was varied logarithmically corresponding to 0.003–0.3 suns in terms of i_{SC}. In these measurements as well as in the steady state *I-V* measurements of the SU–CE cells, the data were recorded with a Zahner Elektrik's IM6 potentiostat. The SU–CE cells were measured at the voltage range of −0.7 to 0.7 V in 5 mV intervals with a 30 s stabilization time for each voltage point. A slow scan rate was required to suppress hysteresis and instability near zero polarization due to double layer charging.

In OCVD measurements, the cells were illuminated using the LED light source while keeping the cells at the open circuit. After the V_{OC} had stabilized, the light was turned off and the decay of the open-circuit voltage was recorded in 50 ms intervals using an Agilent 34970A data logger. The input impedance of the measurement unit was 10 MΩ, and the response time was measured to be less than 40 ms. The OCVD was performed in a black box to avoid stray light.

EIS was performed with Zahner Elektrik's IM6 Impedance Measurement unit over the frequency range of 100 mHz to 100 kHz in the potentiostatic mode using a 10 mV amplitude. The equivalent circuit analysis was made using ZView2 software.

A LI-COR LI-1800 spectroradiometer equipped with an external integrating sphere system was used in the optical measurements in the 390–1100 nm wavelength region. To mimic the situation in the solar cells, the samples consisted of a substrate and a thin microscope glass sealed with a 25 μm thick spacer and filled with 3-methoxypropionitrile.

For the analysis of the surface morphology, a JEOL JSM-7500 scanning electron microscope (SEM) was employed. The X-ray diffraction (XRD) system PANalytical X'Pert PRO MRD was used for an analysis of the crystallinity of the blocking layers. For the same purpose, we also used Zeiss Ultra 55 field emission SEM equipped with a Nordlys II digital electron backscatter diffraction (EBSD) detector and HKL Channel 5 software. In the EBSD measurements, a 10 kV accelerating voltage was employed.

Results and Discussion

Structure of the blocking layers.— Figure 1 shows the SEM images of the TiO_2 blocking-layer-coated samples on the FTO glass substrate and uncoated FTO glass substrates. The conductive coating consists of rather large FTO particles (about 100 nm). Because the 4 nm TiO_2 layer is thin compared to the FTO particle size, it is logical that it has only a very slight smoothing effect on the surface image,

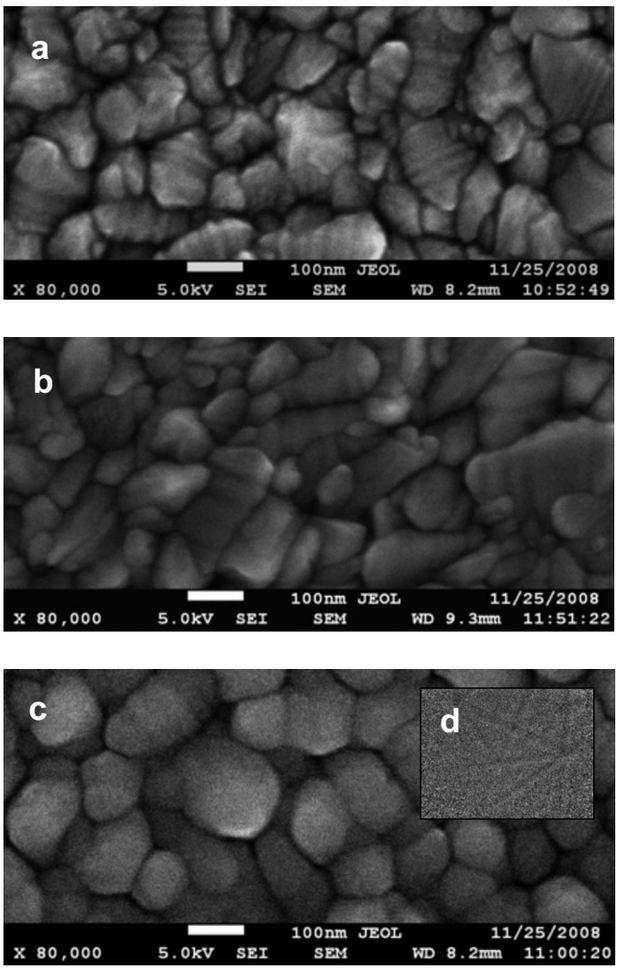

Figure 1. Typical SEM images of (a) uncoated FTO glass, (b) FTO glass with 4 nm TiO_2 layer, and (c) FTO glass with 35 nm TiO_2 layer without temperature treatments. (d) EBSD image of the HT-treated 35 nm TiO_2 blocking layer on plain glass showing Kikuchi lines.

as can be seen when comparing Fig. 1a and b. The 35 nm coating instead changes the surface features by smoothening the shape of the FTO crystal particles, joining neighboring small particles together by filling, and covering the gaps between them (Fig. 1c). In the SEM images, we found no changes between the LT- and HT-treated blocking-layer-coated substrates (data not shown).

ALD blocking layers prepared at LTs are typically amorphous,[17] whereas HT treatments make the films crystalline.[18] We therefore expect that the present ALD TiO_2 layers deposited at 100°C are amorphous but most likely crystallize during the heat-treatment at 450°C used for the sintering of the nanoporous TiO_2 PE film on glass. Efforts were made using several techniques to study the crystallinity of the as-prepared and heat-treated ALD films. Crystallinity is typically studied with XRD, but even the 35 nm thick TiO_2 layers were too thin for the measurement system. However, EBSD analysis showed Kikuchi lines corresponding to the crystal structures of TiO_2 in the HT-treated 35 nm TiO_2 film (Fig. 1d), and in the 35 nm thick LT-treated TiO_2 layer no crystallinity was detected. The 4 nm thick layers were too thin for the EBSD measurement, but they were expected to have similar structures as the thicker films.

Photovoltaic performance.— The HT-treated glass cells produced higher short-circuit current density i_{SC} at 1 sun equivalent illumination and thus also at higher efficiency compared to the LT-treated ITO–PET cells (Fig. 2 and Table I). The positive effect of the

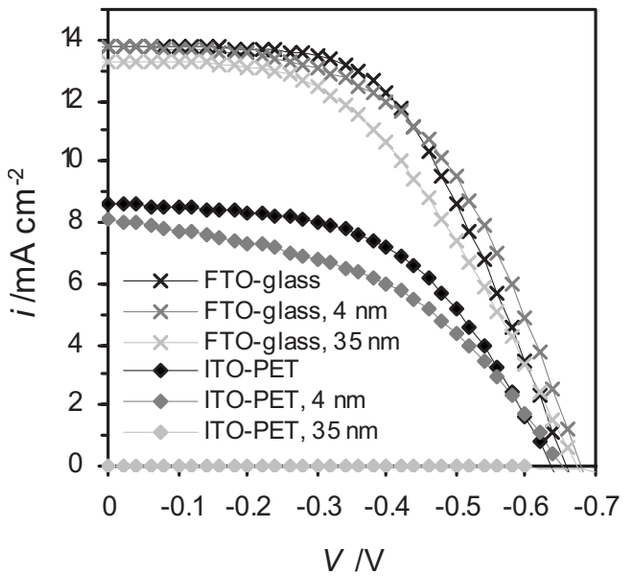

Figure 2. Typical current–voltage curves of the LT-treated ITO–PET and HT-treated FTO glass cells with and without a blocking layer of different thicknesses.

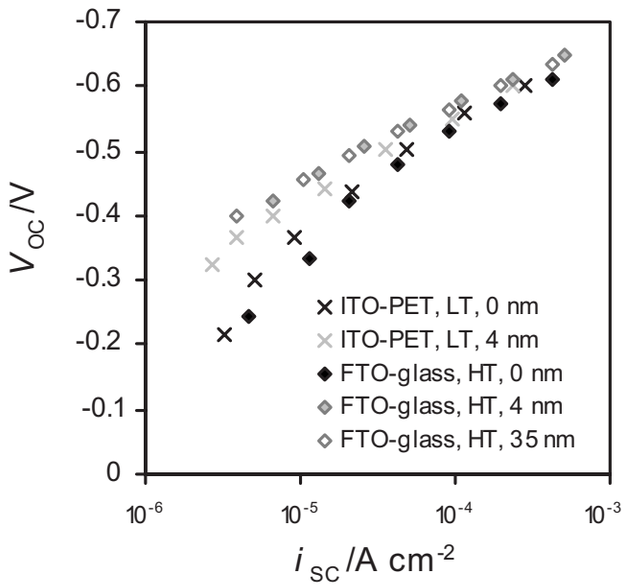

Figure 3. Open-circuit voltage (V_{OC}) of the LT-treated ITO–PET cells and the HT-treated glass cells with and without the TiO_2 blocking layers as a function of short-circuit current density (i_{SC}).

HT treatment of the porous TiO_2 film on the cell performance is well known and is attributed to the light sintering of the particle film yielding improved physical and electrical contact between the TiO_2 nanoparticles. In the LT-treated pressed TiO_2 films, the electron diffusion length is shorter than the film thickness, and thus not all injected electrons are collected, which leads to a lower i_{SC}, as seen in Fig. 2 and Table I. This deduction is supported by the EIS data discussed below.

In 1 sun equivalent illumination, the typical positive impact brought by the blocking layers on the photovoltaic characteristics is the slight increase in V_{OC} (Fig. 2 and Table I). i_{SC} remained about the same in the application of the 4 nm blocking layers, whereas with the 35 nm layers it decreased. Except for the LT-treated cells with the 35 nm layer, these differences in i_{SC} correspond to the decrease in the transmittance of the PE substrate: The 4 nm TiO_2 layer decreased the transmittance by less than 1%, and the 35 nm layer decreased by about 5% in the visible region of both ITO–PET and FTO glass (data not shown).

The blocking layers on ITO–PET decreased the FF clearly, whereas on FTO glass the decrease was very small. The influence of the blocking layers on the *I-V* curve of the ITO–PET cells is similar to what would be expected from a decreased shunt resistance, although this cannot be the actual reason. Considering the two components that contribute the shunt resistance in the cell, namely, the porous TiO_2/electrolyte interface and the substrate/electrolyte interface, the former was similar in all the cells made with the same thermal processing, while the latter only increased when a blocking layer was applied, as indicated by the substrate polarization and EIS measurements discussed below.

The *I-V* curves were similar in both LT- and HT-treated FTO glass cells with the 4 nm blocking layer (data not shown). Contrary to this, LT-treated FTO glass cells with the 35 nm blocking layer (data not shown) showed as poor performance as the ones on ITO–PET with the 35 nm blocking layer. Therefore, the performance loss with the 35 nm layer can be attributed to the LT treatment unlike with the 4 nm blocking layer.

The blocking layer is, however, clearly required to reach high voltage at low light intensities because V_{OC} was increased clearly due to the application of the 4 nm TiO_2 blocking layers in both ITO–PET and FTO glass cells (Fig. 3). Increasing the blocking layer thickness to 35 nm had no impact on the intensity dependence of the V_{OC} in the HT-treated glass cells. The fact that the influence of the blocking layers on V_{OC} becomes more significant toward lower light intensities agrees with literature[6,7,12] and has been linked with substrate-mediated recombination.

The linearity of V_{OC} vs $\log(i_{SC})$ with a slope of 110 mV/decade in the blocking-layer-coated cells (Fig. 3) is indicative of the nonideal diodelike recombination characteristics of the PE, the nonideality factor being ca. 1.8–1.9 in this case. The nonideal diode characteristics of the DSC have been attributed to recombination via the substrate or surface states in the nanoporous TiO_2 film.[19] The re-

Table I. Performance characteristics and their standard deviations for the LT-treated ITO–PET and HT-treated FTO glass cells with and without TiO_2 blocking layers of different thicknesses.

Substrate and blocking layer thickness (nm)	Number of cells	V_{OC} (mV)	i_{SC} (mA cm^{-2})	FF (%)	η (%)
ITO–PET, 0	4	636 ± 9	8.2 ± 0.4	54 ± 1	2.8 ± 0.1
ITO–PET, 4	4	651 ± 9	8.1 ± 0.6	44 ± 2	2.3 ± 0.1
ITO–PET, 35	3	510 ± 70	0.03 ± 0.02	41 ± 4	0.006 ± 0.004
FTO glass, 0	7	642 ± 9	13.8 ± 0.2	52 ± 3	4.6 ± 0.3
FTO glass, 4	4	658 ± 14	13.6 ± 0.1	51 ± 1	4.6 ± 0.2
FTO glass, 35	4	647 ± 25	13.0 ± 0.6	48 ± 4	4.0 ± 0.2

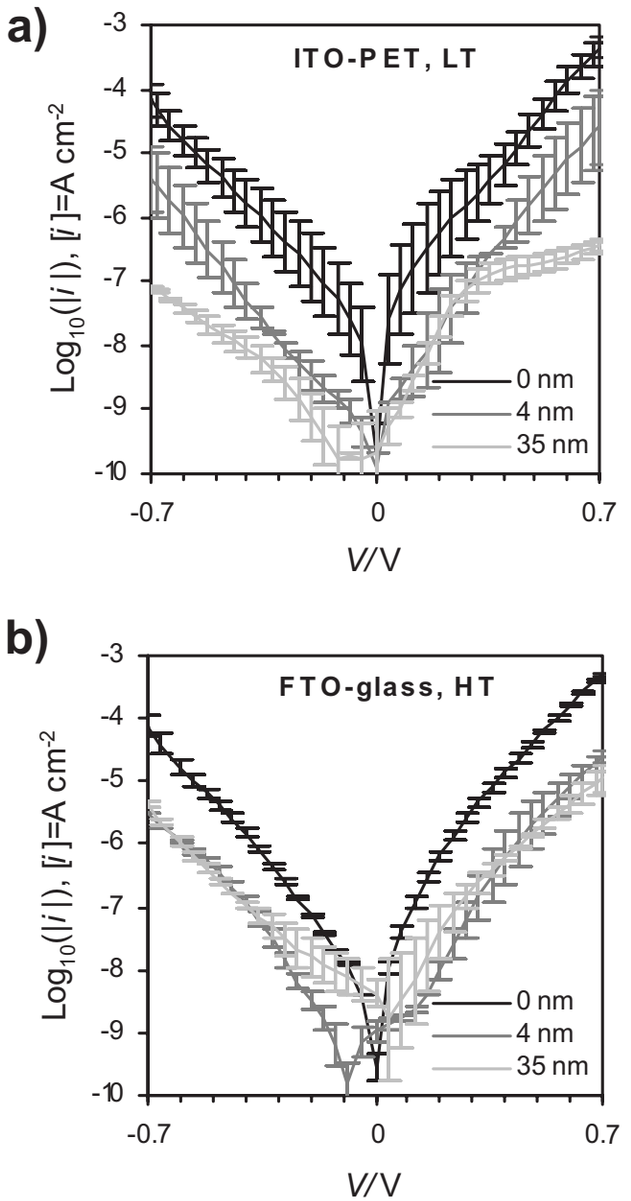

Figure 4. Polarization curves of (a) the bare and the compact TiO_2-coated ITO–PET and (b) FTO glass substrates in the dark. The ITO–PET substrates were treated at LT, and the FTO glass was treated at HT. The error bars indicate standard deviation.

combination via the substrate should be suppressed by the blocking layers, which implies that the nonideality is likely related to recombination via the surface states in this case.

Polarization of the substrate.— Substrate polarization measurements are frequently used for measuring the current leakage from the PE substrate and for verifying the satisfactory performance of the blocking layer. Figure 4 indicates that the recombination currents from both ITO–PET and HT-treated FTO glass substrates were equal. The small effect of the blocking layers at 1 sun illumination can be explained with substrate polarization data: the comparison of the typical DSC i_{SC} (10–20 mA/cm^2) with the recombination current from the bare substrate shows a difference of several orders of magnitude, which suggests that both ITO–PET and FTO glass are as such sufficiently inactive toward tri-iodide reduction reaction at high light intensities.

All the tested blocking layers suppressed the current by about 1 decade throughout the studied voltage range compared to the bare substrate except for the 35 nm layer on ITO–PET, which decreased it even more. This is due to the LT treatment: LT-treated FTO-glass cells with the 35 nm layer (data not shown) are presented as low currents as the ITO–PET cells with the 35 nm layer.

Compared to the previous results,[7-9,13] the data in Fig. 4 demonstrate excellent recombination blocking characteristics: For the heat-treated FTO glass substrates, the recombination currents were 1–2 decades smaller, and for the substrates with blocking layer similar or lower than reported previously.

OCVD.— OCVD is an efficient technique for a quantitative study of electron transfer at the PE. In the OCVD, the gradual loss of photogenerated electrons due to recombination is monitored by measuring the transient decay of the cell voltage after switching off the light. Because the cell is kept at an open circuit during the experiment, the data are not obscured by the transient response by other cell components and the measured voltage can be assigned solely to the PE. From the transient data, the effective electron lifetime τ_{eff} is obtained as[20]

$$\tau_{eff} = -\frac{k_B T}{e}\left(\frac{dV_{OC}}{dt}\right)^{-1} \quad [1]$$

where k_B is the Boltzmann coefficient, T is the temperature, e is the elementary charge, and t is the time. Note that the OCVD data of the blocking-layer-coated solar cells in Fig. 5 should be interpreted qualitatively for voltages less negative than −0.2 V where the input impedance of the measurement device may not be significantly larger than the charge-transfer resistance of the PE/electrolyte interface (Fig. 10).

The blocking layers increased the electron lifetime primarily at the small negative voltage, as shown in Fig. 5. This result agrees with literature.[21,22] According to literature,[21,22] the electron lifetimes at large negative voltages correspond to the porous TiO_2 layer and they should be similar for similarly prepared films. This was seen with both LT-treated (Fig. 5) and HT-treated FTO glass cells. Interestingly, the application of the 4 nm blocking layer on the ITO–PET caused an increase in τ_{eff} also at the large negative voltages.

The LT-treated cells with the 35 nm layer gave high electron lifetimes. These cells also illustrated a very low current in the substrate polarization measurements. The photovoltaic performance of these cells was, however, very poor. This demonstrates the fact that while OCVD and polarization measurements are useful to clarify interfacial charge transfer in DSC, they do not provide all the necessary information to explain the photovoltaic cell performance. For this, techniques sensitive to the charge transport in the cell are also needed. EIS is one of the most effective techniques for this purpose.

EIS response and equivalent circuit fitting.— Sintering of the PE layer has a significant effect on the EIS response of the cell because it notably decreases the transport resistance in the TiO_2 film. Hence, to see the effect of the substrate instead of the temperature treatment, we primarily discuss the data of the LT-treated cells in the EIS analysis. A separate remark is made if the data are from the HT-treated cells.

The general equivalent circuit of a DSC similar to the one presented by Fabregat-Santiago et al.[23] is illustrated in Fig. 6. Constant phase elements (CPEs) are used instead of pure capacitors as they better describe the uneven and porous electrodes. The circuit in Fig. 6 can be approximated with simplified circuits depending on the voltage.[21] From −0.1 to −0.3 V, only one semicircle corresponding to the PE could be detected in the low frequencies, and in the data fitting equivalent circuit (a) (Fig. 7) was employed. From −0.4 to −0.7 V, the PE showed a Gerischer-type response,[21] and there was at least one semicircle detectable at the higher frequencies (Fig. 8). For the data fitting of these data, equivalent circuit (b) (Fig. 7) was used. In the Gerischer-type response only the upper limit for R_{CT}

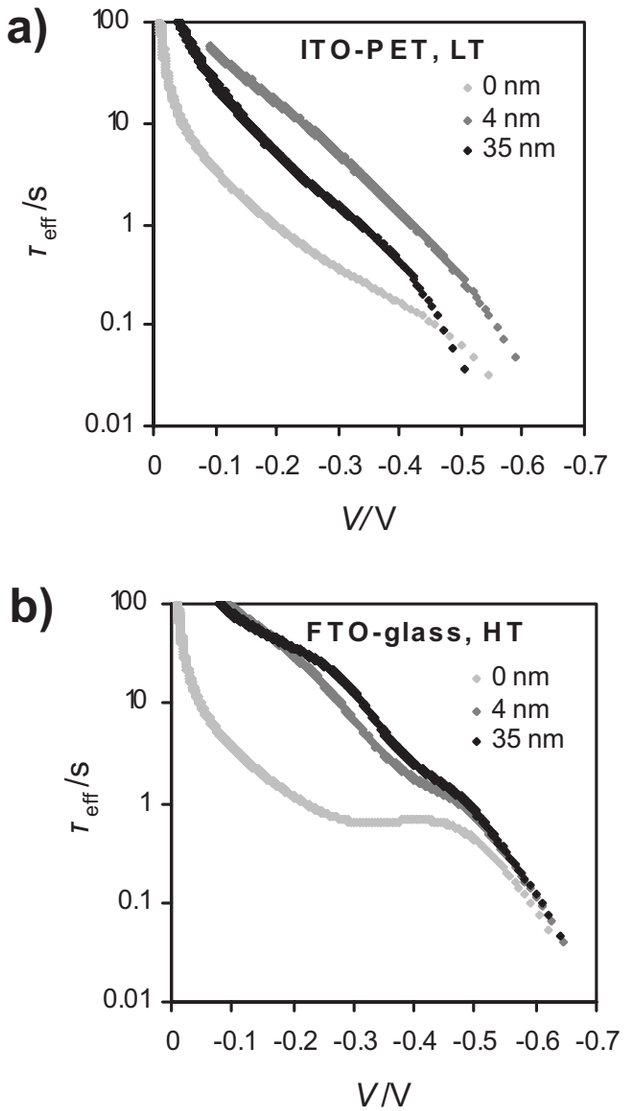

Figure 5. Typical effective electron lifetime of LT-treated solar cells deposited on (a) ITO–PET and (b) HT-treated FTO glass with and without a compact TiO_2 layer.

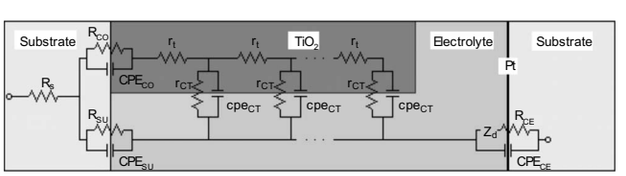

Figure 6. General equivalent circuit model of a DSC similar to the one presented by Fabregat-Santiago et al.[23] R_s is the Ohmic series resistance caused by sheet resistance of the substrates, current collector contacts, etc. CPE_{SU} and R_{SU} are the CPE and charge-transfer resistance at the PE substrate/electrolyte interface. CPE_{CO} and R_{CO} are the CPE and charge-transfer resistance between the PE substrate and the porous TiO_2. R_t ($=r_t d$) is the electron-transport resistance, and d is the thickness of the layer. CPE_{CT} ($=CPE_{CT}/d$) and R_{CT} ($=r_{CT}/d$) are the CPE and the charge-transfer resistance at the TiO_2/electrolyte interface. Z_d is the mass transfer impedance at the counter electrode due to ionic diffusion in the electrolyte. CPE_{CE} and R_{CE} are the CPE and charge-transfer resistance at the counter electrode/electrolyte interface.

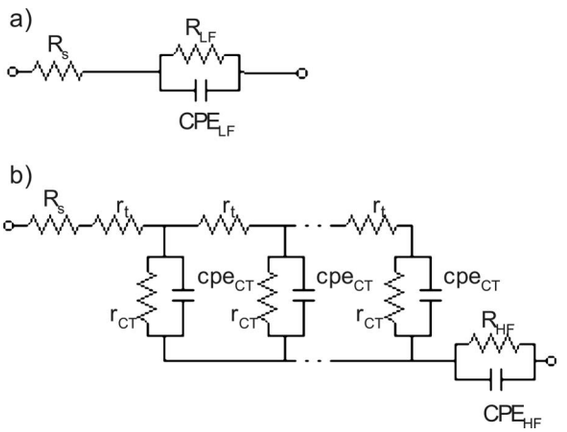

Figure 7. Equivalent circuits used in the data fitting (a) in the case where transport resistance in the TiO_2 could be omitted and (b) in the case where it could be included. CPE_{LF} and R_{LF} mark for the EIS component detected in low frequencies, which depending on the voltage can be linked to different PE/electrolyte interfaces or PE components. CPE_{HF} and R_{HF} correspond to the charge-transfer components observed at high frequencies, which, in practice, are CPE_{CE} and R_{CE} or CPE_{CO} and R_{CO}.

can be estimated, as explained in the Appendix. For SU–CE cells, there was one semicircle present throughout the studied voltage range, and equivalent circuit (a) was used.

The blocking layer brings along additional R/CPE components, which may contribute to the EIS response. Indeed, the presence of at least one such component was detected. In the most general case, the impedance of the blocking-layer-coated substrates can be considered to consist of three series connected R/CPE couples between the conductive coating of the substrate [transparent conducting oxide (TCO)] and the porous TiO_2 film: the substrate/compact TiO_2 interface $R_{TCO/BL}$, the compact TiO_2 bulk layer R_{BL}, and the compact TiO_2/porous TiO_2 interface R_{BL/TiO_2}. In the blocking-layer-coated samples, we denote the sum of these resistances with R_{CO}, whereas R_{SU} consists of the series connection of the substrate/compact TiO_2 interface, the compact TiO_2 bulk layer, and the compact TiO_2/electrolyte interface $R_{BL/EL}$

$$R_{CO} = R_{TCO/BL} + R_{BL} + R_{BL/TiO_2} \quad [2]$$

$$R_{SU} = R_{TCO/BL} + R_{BL} + R_{BL/EL} \quad [3]$$

Typically, a conducting homogeneous bulk layer functions as a simple resistor without a capacitive component. However, a thin compact TiO_2 blocking layer can be alternatively regarded as an insulator between two conductive layers, and hence its impedance could be equivalent to a leaking parallel plate capacitor. The capacitance of the blocking layer C_{BL} can then be estimated as

$$C_{BL} = \varepsilon_r \varepsilon_0 \frac{A}{d_{BL}} \quad [4]$$

where ε_r is the relative permittivity of the blocking layer material, ε_0 is the vacuum permittivity, A is the area of the layer, and d_{BL} is the thickness of the layer.

According to the EIS measurements, the presence of a blocking layer had only a very slight impact on the Ohmic resistance R_s of the cell. The ALD coating did not have a marked impact on the sheet resistance of the conducting oxide coating of the substrates.

High frequency EIS response.— The width of the high frequency semicircle R_{HF} on the left in Fig. 8a is usually attributed to charge transfer at the counter electrode R_{CE}. The differences in the width of the high frequency semicircle R_{HF} on the left in Fig. 8a can be quantitatively compared by analyzing the data as a function of external current (Fig. 9), as described in our previous work.[11] R_{HF} is

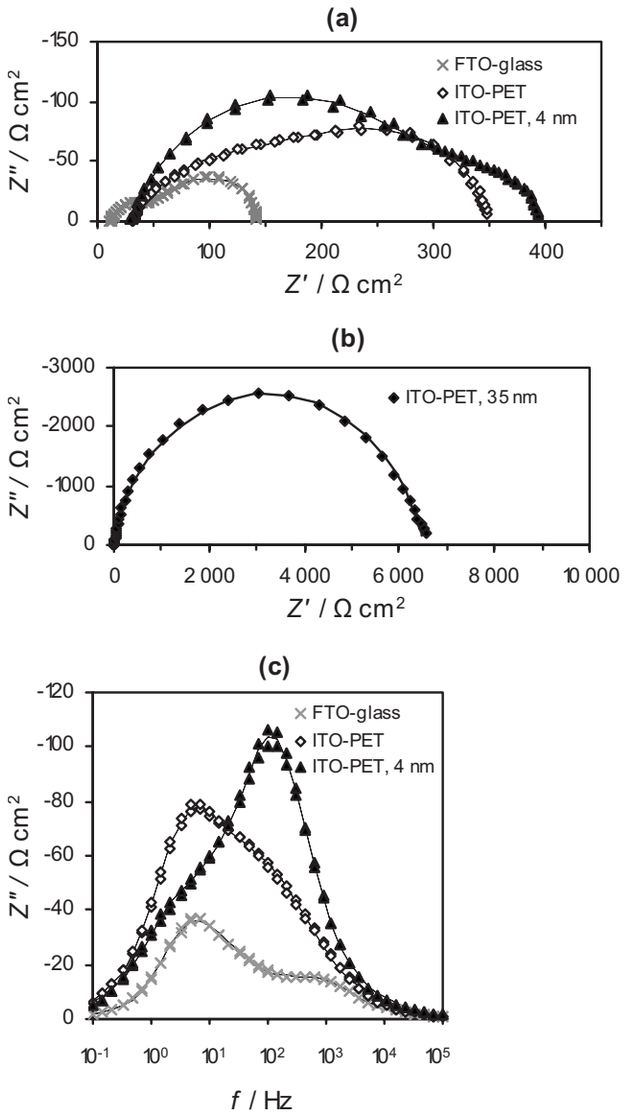

Figure 8. Sample EIS data of DSCs with LT-treated PEs at −0.6 V in the dark. Imaginary impedance vs real impedance of (a) FTO glass, ITO–PET, and ITO–PET with 4 nm blocking layer and (b) ITO–PET with 35 nm blocking layer. (c) Imaginary impedance vs frequency. The markers refer to the measured data and the continuous lines to the fitted data.

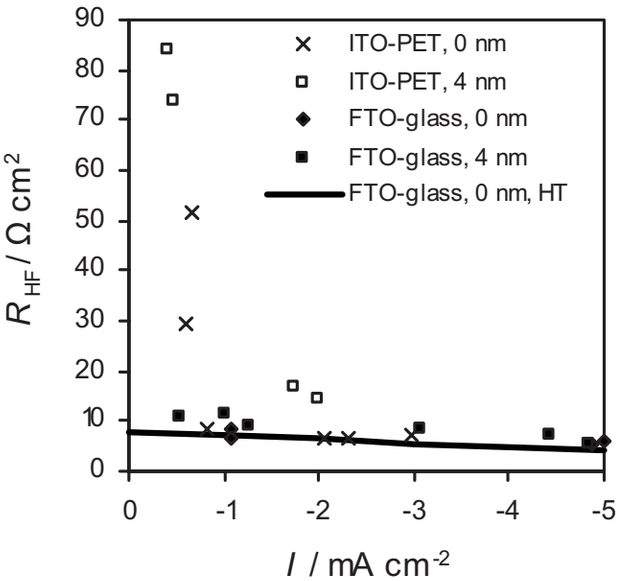

Figure 9. Resistance of the high frequency impedance component R_{HF} of the LT-treated solar cells with and without blocking layer in comparison to that of the cells with HT-treated PE on FTO glass.

usually attributed to charge transfer at the counter electrode R_{CE}. In agreement with this, in the FTO glass solar cells, R_{HF} equaled R_{CE} measured in symmetric CE–CE cells (data not shown). It can therefore be concluded that the high frequency response of the FTO glass cells is governed by the charge transfer at the counter electrode.

Interestingly, Fig. 9 shows that the R_{HF} of the ITO–PET cells is much higher compared to those of the FTO glass cells although the counter electrodes should have shown equal performances due to their similar preparation. When R_{CE} is subtracted from R_{HF}, a significant impedance component remains. The dependence of R_{HF} on the PE substrate suggests that the remaining component is caused by R_{CO}. A similar increase in R_{HF} has also been previously detected in a smaller scale when using different substrates.[24]

The presence of the 4 nm layer on ITO–PET increased R_{HF} even further. In the LT-treated cells with the 35 nm layer, there was only a single large semicircle which was at least an order of magnitude larger than the total resistance of the uncoated cells at the corresponding voltages, as depicted for a voltage −0.6 V in Fig. 8a and b.

Because both the counter electrodes and the porous TiO_2 layers in the cells should be similar with and without a blocking layer, the presence of a very large semicircle suggests that the R_{CO} dominates the response and overlaps not only with R_{CE} but also with R_{CT} in those cells.

For the glass cells, R_{CE} was of the same magnitude as R_s and Z_d (data not shown), which together form the resistance that decreases the FF in the photovoltaic measurements. R_{CO} values measured here for ITO–PET cells are larger than R_{CE}, and therefore they are expected to have an observable impact on the slope of the *I-V* curve near the open-circuit state and also on the FF. The R_{CO} of the 35 nm layer ITO–PET cells is so large that it is expected to flatten the *I-V* curve to the extent that it lowers i_{SC} significantly. In agreement with this, the *I-V* curves of the ITO–PET cells without a blocking layer have a steeper slope compared to the ones with the blocking layers and suppressed i_{SC} in the case of the 35 nm layer (Fig. 2 and Table I). Note that the R_{CO} was voltage dependent, which causes the *I-V* curve of the LT-treated 35 nm coated solar cells to deviate from a straight line. In the LT-treated SU–CE cells with the 35 nm layer, it is likely that R_{CO} had a marked contribution to the low current seen in the polarization measurements (Fig. 4). In other substrate/blocking layer combinations, the other resistances were significantly smaller than those of the blocking layer/electrolyte interface, and the lowering of the leakage current in Fig. 4 can be attributed to an actual decrease in electron recombination.

The blocking layers produce three possible EIS components that can be linked with the increased R_{CO}. If the bulk resistance of the compact blocking layer were to contribute to the high frequency impedance arc corresponding to R_{CO}, the dielectric capacitance of the blocking layer (Eq. 4) would have to be of the same order of magnitude as the measured capacitance C_{CO}. Using the relative permittivity of TiO_2 varying from 25 to 100, which is a larger range than that typically observed for TiO_2 thin films,[17,25] the dielectric capacitance of the 4 nm blocking layer was calculated to range from 2×10^{-6} to 7×10^{-6} F. The measured value for cells with the 4 nm blocking layer on ITO–PET was approximately 2×10^{-5} F. Because the C_{CO} values do not correspond and because the material difference between the compact TiO_2/porous TiO_2 should not be significant, the increased R_{CO} is most likely due to the resistance at the ITO/compact TiO_2 interface in the ITO–PET cells with the 4 nm

layer. In the LT-treated cells with the 35 nm blocking layer, the measured capacitance varied from 7×10^{-7} to 2×10^{-6} F, which partly matches with the calculated C_{BL} values that range from 2×10^{-7} to 8×10^{-7} F. Hence, for the LT-treated 35 nm films, a contribution from the bulk resistance of the blocking layer on the measured R_{HF} cannot be ruled out.

It would be logical that the thickening of the blocking layer would increase the bulk resistance. The effect does not, however, appear in the HT-treated cells. The HT treatment apparently induced a structural change in the TiO_2 blocking layers from amorphous to crystalline. It is likely that the improved conductivity seen in the EIS measurements is linked with the structural change from amorphous to crystalline. This could be understood by current transport being more difficult in a material in a disorganized (amorphous) structure than in one in which there is a deviation from the organized structure only in the grain boundaries. Amorphous TiO_2 films are therefore expected to be less conductive than crystalline ones. As a result, the amorphous 35 nm TiO_2 layer appears to have been too thick, whereas the amorphous 4 nm layer was thin enough to function as a blocking layer in DSCs; in the crystalline TiO_2 layer obtained by the heat-treatment, even the 35 nm thick layers were thin enough to provide sufficiently low resistance. Even the crystalline compact TiO_2 layers become too resistive as the film thickness is increased enough. For instance, with sputtered films, the film was too resistive when its thickness exceeded approximately 200 nm.[9] Apparently, thicker ALD layers can be used in the HT-treated cells than in the LT cells.

PE EIS response.— The resistance connected to the low frequency EIS response (R_{LF}) for solar cells and SU–CE cells prepared using a LT treatment is displayed in Fig. 10. It was estimated that in Fig. 10 the external cell voltage differs from the voltage over the PE only in the presence of the porous TiO_2 layer at voltages more negative than −0.4 V and at most by some tens of millivolts. Hence, the voltage corrections such as those employed in Ref. 11 were omitted here as they would not have resulted in any changes in the main conclusions. The 35 nm blocking-layer-coated cells are omitted here as they were already discussed above.

The presence of the 4 nm thick blocking layer increased the recombination resistance of the SU–CE cells approximately 1–2 orders of magnitude. This result is equivalent to the substrate polarization measurements, as to be expected because the EIS results show the derivative of the polarization curve. In the complete solar cells, the 4 nm blocking layer significantly increased the recombination resistance at small negative potentials (Fig. 10). This result is in good correspondence with the OCVD data and the low light intensity measurements, which both showed improved performance at small negative potentials. The OCVD data and the EIS data are also linked because the effective electron lifetime τ_{eff} (Fig. 5) is the product of the corresponding resistance (Fig. 10) and capacitance.[26]

At the high negative potentials, a transmission line feature characteristic of a porous electrode film could be detected. At that voltage region, the EIS response corresponds to the recombination from the porous TiO_2 layer, and because the layers should be similar in all the cells in Fig. 10, their similar performances are an expected result. As the recombination resistance of the 4 nm blocking-layer-coated substrate substantially increased the substrates' recombination resistance (Fig. 10), the recombination current flows through the porous TiO_2 also at the smaller voltages in those cells.

The recombination resistance of the uncoated solar cells repeatedly showed smaller values approximately 1 order in magnitude compared to the SU–CE cells, the performance of which should correspond to that of the PE substrate. This observation contradicts the result of Fabregat-Santiago et al., who found that the PE resistance of a solar cell equaled the recombination resistance of the substrate at small negative voltages.[21] Finally, we point out that the data in Fig. 10 cannot be explained with a simple parallel connection of the porous TiO_2 layer with the substrate (Fig. 6) even when taking into account the effect of the substrate/TiO_2 interface in the small negative voltages. This suggests that there might be some kind of interaction between the substrate and the TiO_2 layer that the EIS model cannot explain because it considers the components to be independent.

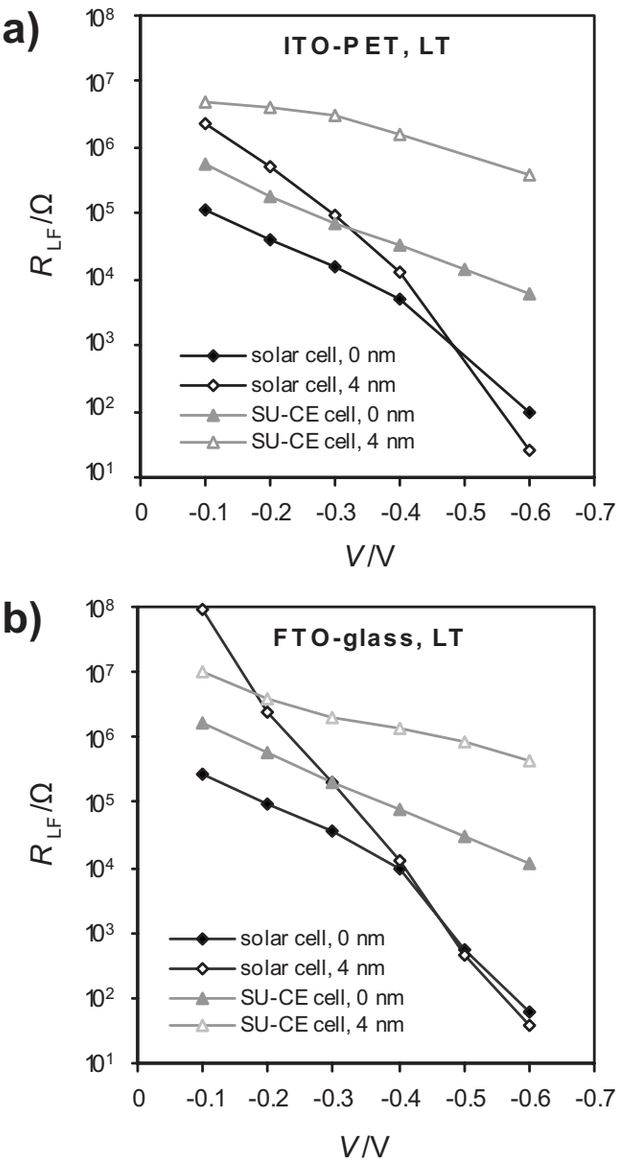

Figure 10. Typical solar cell and SU–CE cell and substrate resistances of LT-treated (a) ITO-PET and (b) FTO-glass cells. In the samples that contain porous TiO_2, only the upper limit of R_{LF} could be determined at the voltages more negative than −0.4 V due to the Gerischer-type response.

Conclusions

LT ALD TiO_2 blocking layers were applied on ITO–PET PE substrates, and their electrochemical performance was examined using multiple complementary techniques. The recombination from the ITO–PET substrate is on a similar level than that from the FTO glass substrates. At high light intensities, both ITO–PET and FTO glass were sufficiently resistant toward recombination even without blocking layers. The blocking layers proved to be useful, however, in gaining high open-circuit voltages at low light intensities.

The other resistance components introduced by the blocking layer in addition to the recombination resistance were shown to be important: In the ITO–PET cells with the 4 nm blocking layer, a

high frequency impedance component was found in the EIS and attributed to the contact resistance between the ITO and the compact TiO_2. In the LT-treated cells with the 35 nm layer, an even larger resistance was detected and it appeared to be dominated by the bulk resistance of the TiO_2 blocking layer.

As the difference between HT- and LT-treated 35 nm layers showed, temperature treatments have a profound effect on the performance of the blocking layer. The effect was linked with improved conductivity due to a structural change from amorphous to crystalline in the heat-treatment. In practice, this suggests that in this type of film thicker layers can be employed in HT-treated cells, whereas LT-treated cells require thinner ones. Hence, the blocking layers need to be separately optimized for LT-treated DSCs by the minimization of FF losses due to the resistivity of the blocking layer while maintaining low recombination resistance.

It is clear that work is still required to better understand the phenomena at the interfaces and in the bulk of the blocking layer. In that work, the investigation of the electronic structure between each layer, such as bandgap and energy-level alignment, should be useful.

Acknowledgment

The support of the Finnish Funding Agency for Technology and Innovation (Tekes) is acknowledged. K.M. is grateful for the scholarship from the Graduate School of Energy Technology. We thank Planar Systems, Inc. (Nora Isomäki, currently Beneq Oy) for the ALD blocking layers. We also thank Juuso Korhonen (Department of Applied Physics, TKK) for the SEM images and Pasi Kostamo (Department of Micro and Nanosciences, TKK) for the XRD measurements. This work used the facilities of Helsinki University of Technology, Nanomicroscopy Center (TKK-NMC).

Helsinki University of Technology assisted in meeting the publication costs of this article.

Appendix

Interpretation of the Gerischer-Type Impedance Response

The low frequency end of the Gerischer response is a semicircle, while the high frequency end displays a 45° slope in the complex plane. The Gerischer response corresponds to a situation where the electron-transport resistance is equal to or higher than the recombination resistance of the PE film, and thus the electron diffusion length L is smaller than the film thickness d. In such a case, R_{CT} and R_t cannot be determined independently by equivalent circuit fitting because in this case the transmission line model reduces to the Gerischer impedance that is characterized by only one independent resistance parameter, the Gerischer resistance $R_G = (R_{CT}R_t)^{1/2}$, which corresponds to the total width of the impedance arc.[21] However, using the additional information that the Gerischer response is observed only when $R_{CT} < R_t$ (approximately), the upper limit $R_{CT,max}$ and the lower limit $R_{t,min}$ can be determined: Fitting a semicircle to the low frequency end of the spectrum yields an estimate of $R_{CT,max}$. Any larger R_{CT} value than this, which is also consistent with the total width of the impedance arc, would not result in a Gerischer impedance but an R_t slope and an R_{CT} semicircle would be separated in the EIS spectrum, as described by the transmission line impedance model.

References

1. H. Lindström, A. Holmberg, E. Magnusson, S. Lindquist, S. Malmqvist, and A. Hagfeldt, *Nano Lett.*, **1**, 97 (2001).
2. T. Miyasaka, M. Ikegami, and Y. Kijitori, *J. Electrochem. Soc.*, **154**, A455 (2007).
3. M. G. Kang, N.-G. Park, K. S. Ryu, S. H. Chang, and K.-J. Kim, *Sol. Energy Mater. Sol. Cells*, **90**, 574 (2006).
4. S. Ito, N.-L. C. Ha, G. Rothenberger, P. Liska, P. Comte, S. M. Zakeeruddin, P. Péchy, M. K. Nazeeruddin, and M. Grätzel, *Chem. Commun. (Cambridge)*, **38**, 4004 (2006).
5. Y. Jun, J. Kim, and M. G. Kang, *Sol. Energy Mater. Sol. Cells*, **91**, 779 (2007).
6. S. Hore and R. Kern, *Appl. Phys. Lett.*, **87**, 263504 (2005).
7. P. J. Cameron, L. M. Peter, and S. Hore, *J. Phys. Chem. B*, **109**, 930 (2005).
8. J. Xia, N. Masaki, K. Jiang, and S. Yanagida, *J. Phys. Chem. B*, **110**, 25222 (2006).
9. J. Xia, N. Masaki, K. Jiang, and S. Yanagida, *J. Phys. Chem. C*, **111**, 8092 (2007).
10. R. Hattori and H. Goto, *Thin Solid Films*, **515**, 8045 (2007).
11. K. Miettunen, J. Halme, M. Toivola, and P. Lund, *J. Phys. Chem. C*, **112**, 4011 (2008).
12. A. Burke, S. Ito, H. Snaith, U. Bach, J. Kwiatkowski, and M. Grätzel, *Nano Lett.*, **8**, 977 (2008).
13. P. J. Cameron and L. M. Peter, *J. Phys. Chem. B*, **107**, 14394 (2003).
14. H. Lindström, E. Magnusson, A. Holmberg, S. Södergren, S. Lindquist, and A. Hagfeldt, *Sol. Energy Mater. Sol. Cells*, **73**, 91 (2002).
15. N. Papageorgiou, W. F. Maier, and M. Grätzel, *J. Electrochem. Soc.*, **144**, 876 (1997).
16. S. Ito, K. Nazeeruddin, P. Liska, P. Comte, R. Charvet, P. Péchy, M. Jirousek, A. Kay, S. Zakeeruddin, and M. Grätzel, *Prog. Photovoltaics*, **14**, 589 (2006).
17. G. D. Wilk, R. M. Wallace, and J. M. Anthony, *J. Appl. Phys.*, **89**, 5243 (2001).
18. J. Aarik, A. Aidla, A.-A. Kiisler, T. Uustare, and V. Sammelselg, *Thin Solid Films*, **305**, 270 (1997).
19. L. M. Peter, *J. Phys. Chem. C*, **111**, 6601 (2007).
20. A. Zaban, M. Greenshtein, and J. Bisquert, *ChemPhysChem*, **4**, 859 (2003).
21. F. Fabregat-Santiago, J. Bisquert, G. Garcia-Belmonte, G. Boschloo, and A. Hagfeldt, *Sol. Energy Mater. Sol. Cells*, **87**, 117 (2005).
22. P. J. Cameron and L. M. Peter, *J. Phys. Chem. B*, **109**, 7392 (2005).
23. F. Fabregat-Santiago, J. Bisquert, E. Palomares, L. Otero, D. Kuang, S. M. Zakeeruddin, and M. Grätzel, *J. Phys. Chem. C*, **111**, 6550 (2007).
24. T. Hoshikawa, M. Yamada, R. Kikuchi, and K. Eguchi, *J. Electrochem. Soc.*, **152**, E68 (2005).
25. S. Duenãs, H. Castán, H. Garciá, E. San Andrés, M. Toledano-Luque, I. Mártil, G. Gonzáles-Díaz, K. Kukli, T. Uustare, and J. Aarik, *Semicond. Sci. Technol.*, **20**, 1044 (2005).
26. J. Bisquert, G. Garcia-Belmonte, F. Fabregat-Santiago, N. S. Ferriols, P. Bogdanoff, and E. C. Pereira, *J. Phys. Chem. B*, **104**, 2287 (2000).